Modeling on the feasibility of camera-based blood glucose measurement

Yiyin Wang
Eindhoven University of Technology
wangyiyin99@gmail.com

Wenjin Wang
Philips Research
wenjin.wang@philips.com

Mark van Gastel
Philips Research
mark.van.gastel@philips.com

Gerard de Haan
Eindhoven University of Technology
g.d.haan@tue.nl

Abstract

Monitoring of blood glucose levels is crucial for diabetics to manage their lives. However, the current gold-standard requires taking invasive blood samples, which is painful and can lead to infections. In this paper, we investigate the feasibility of using a regular camera (with silicon image sensors) to estimate the blood glucose levels remotely as claimed by recent studies. The physiological challenge is the small volume fraction and low absorption of glucose in the human body as compared to other absorbers. The glucose-induced variations in light intensity from both the non-pulsating and the pulsating part of the reflected optical signal are modeled in the visible to near-infrared wavelength range. The simulation results suggest that it is unlikely to detect the blood glucose based on either the DC or AC component of skin reflected light. The optical responses caused by glucose changes are minor as compared to other physiological factors (e.g. skin temperature, SaO_2, water concentration). This, combined with the coarse sampling of the light spectrum by regular cameras render the measurement infeasible.

1. Introduction

In 2015, 415 million adults have been diagnosed as diabetics worldwide and the number of diabetics is estimated to increase to 642 million in 2040 [8]. Diabetes has become one of the most severe health treats in the 21st century. Monitoring of blood glucose can help people to manage the life-style by adjusting their food intake or physical exercises. Moreover, diabetics can verify the effectiveness of the former insulin dose and make a decision for the next insulin dose [16]. The approaches for glucose measurement can roughly be divided into two categories: invasive and non-invasive. The invasive approach draws blood from a person's body using a lancet device and applies it to a "test-strip" to determine the blood glucose concentration by measuring electrical characteristics [16]. Despite the fact that the invasive approach can provide an accurate measurement of blood glucose levels, it is very obtrusive and painful, and can also cause infection. To solve this problem, non-invasive optical techniques have been proposed, such as Fluorescence Spectroscopy [1, 19], Raman Spectroscopy [26] and NIR Spectroscopy [27, 23]. Although these techniques reported promising results, most of them require bulky and expensive equipment, rendering the daily usage impossible. To reduce the cost, a machine-learning approach using features extracted from the photoplethysmographic (PPG) waveform has been proposed by Monte-Moreno [18] to estimate blood glucose levels, which was combined with other features like age, weight and BMI.

Recent studies claim that it is possible to measure the blood glucose levels from a smart-phone camera and a spectrophotometer [4, 5, 22]. Dantu *et al.* used 650 nm light and a HTC One X Android phone camera to estimate blood glucose levels based on the finger transmitted light [4, 5]. Their study shows that the skin color changes are related to the blood glucose changes. Uwadaira *et al.* studied the glucose-linked wavelengths where the light intensity is strongly correlated with the glucose concentration in short near-infrared spectra (700-1050 nm, 1 nm intervals) [22], which is within the sensitivity of most silicon-based sensors. Based on 300 measurements from 30 volunteers, they found five glucose-linked wavelengths according to the variations in the absorption of glucose in the spectra. They also mentioned that the glucose-linked wavelengths fluctuate daily even for the same person.

Because of the low concentration of glucose and its low absorption in visible and near-infrared wavelengths [28], we however question whether it is really possible to detect changes in glucose-levels with a regular camera. We therefore perform a mathematical modeling on (optical) camera-based blood glucose measurement to investigate its feasibil-

ity from a theoretic perspective, focussed on the more practical and common reflective mode measurement, rendering its usage not limited to relative thin skin sites such as fingers and ear lobes. The modeling consists of two parts: the DC-component based glucose measurement and AC-based glucose measurement. We expect the principal challenge to be the minor optical responses caused by glucose changes as compared to other physiological factors. Our hypothesis is that the variations of other stronger absorbing components in the visible to near-infrared wavelength range (e.g. (oxy)hemoglobin, water) and body temperature can create significant interference for *in vivo* glucose measurements.

2. Opto-physiological modeling of glucose

In this section, we use opto-physiological mathematical modeling of the light propagation in tissues to investigate the influence of glucose changes on both the DC and AC components of the camera PPG waveform. In addition, the influence of changes in body temperature, water concentration and SaO_2 are studied through the model.

2.1. DC component modeling

Since the prior art based on DC measurement [4, 5] use finger-transmitted light, our DC component modeling assumes the skin transmission measurement. The principles of PPG can be modeled by Beer-Lambert law, which states that in a homogeneous medium, light intensity decays exponentially as a function of path length and light absorption coefficient corresponding to medium properties at a specific wavelength. The scattering coefficient has a much larger influence than the absorption coefficient on the light propagation in the tissue in the range of visible and short near-infrared wavelengths. Based on the diffusion approximation [12] [7], we can use below equation to model *in vivo* glucose measurements:

$$I(\lambda) = I_0(\lambda) e^{-\sum_{i=1}^{n} \mu_{eff}^{(i)}(\lambda) l^{(i)}} \tag{1}$$

where

$$\mu_{eff}^{(i)}(\lambda) = \sqrt{3\mu_a^{(i)}(\lambda)(\mu_a^{(i)}(\lambda) + \mu_s'^{(i)}(\lambda))}, \tag{2}$$

where $I_0(\lambda)$ is the intensity of incident light at the wavelength λ, $I(\lambda)$ is the intensity of transmitted light obtained from a camera at the wavelength λ, $\mu_a^{(i)}(\lambda)$ and $\mu_s'^{(i)}(\lambda)$ are the absorption coefficient and scattering coefficient for seven layers at the wavelength λ, $l^{(i)}$ is the optical path length in seven layers, and i denotes the skin-layer index. A detailed description of the coefficients is provided in the next subsection.

2.1.1 Skin layer structure

To perform opto-physiological model simulations, one first needs to model the various skin layers. Skin presents a complex medium, because the distribution of blood and chromophores vary with depth. The absorption and reduced scattering coefficients of different skin layers are also different. According to [17], skin can be divided into seven layers (see Fig. 1). The first layer is known as the stratum corneum which is the outermost of epidermis layer. The second layer is defined as living epidermis which contains living cells such as melanosomes, columnar cells and small melanin granules [7]. These two layers have no blood. The distribution of blood is different in the dermal layer, which is subdivided into four different layers. These are the papillary dermis layer, upper blood net dermis layer, reticular dermis layer, and deep blood net dermis layer [17]. The bottom layer is the subcutaneous fat layer in our model. Since the thickness and distribution of layers vary for the different skin regions of a human body and different individuals, the skin modeling may not be realistic enough to present the complex human skin structure and not accurate enough for measurement calibration. We mention that the main purpose of the skin modeling is to help us study the light intensity changes caused by glucose variations compared to that caused by variations of other factors such as body temperature, water concentration and SaO_2.

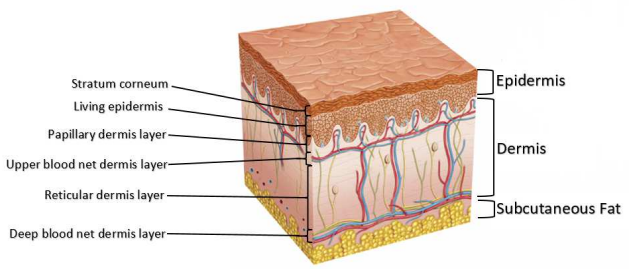

Figure 1. The skin model used for modeling contains seven layers.

The volume fraction of glucose is expressed as:

$$V_g = \frac{C_g}{\rho_g}, \tag{3}$$

where C_g is the concentration of glucose in the blood and ρ_g is the density of glucose. The volume fractions of blood (V_{blood}) and water (V_{H_2O}) are shown in Table 1 [17, 20]:

Moreover, the volume fraction of water in the dermis layer and the subcutaneous fat layer have been split into three parts: water in the interstitial fluid (IF), water in the blood plasma, and water in the intracellular fluid (ICF). The volume fraction of water in the IF is 4 times higher that of plasma. The volume fraction of extracellular fluid (ECF) which is composed by IF and blood plasma that is 33% of human body [2]. We assume that water concentration $C_w = 540\ g/l$ is identical in the three parts. Furthermore, the water concentrations in the IF and in the blood plasma decrease when glucose increases. The concentration

Name of layer	V_{blood}	V_{H_2O}
Stratum corneum	0	0.05
Living epidermis	0	0.2
Papillary dermis	0.04	0.5
Upper blood net dermis	0.3	0.6
Reticular dermis	0.04	0.7
Deep blood net dermis	0.1	0.7
Subcutaneous fat	0.05	0.7

Table 1. The used volume fractions of blood and water in seven different skin layers.

of water in ICF is not affected by the glucose concentration. Therefore:

$$V_{w_{plasma}} = \frac{C_w}{\rho_w} V_{blood}, \tag{4}$$

$$V_{w_{IF}} = 4\frac{C_w}{\rho_w} V_{blood}, \tag{5}$$

$$V_{w_{ICF}} = 0.67 V_w. \tag{6}$$

The volume fraction of haemoglobin is defined as:

$$V_{Hb} = F_{Hb} F_{RBC} Ht V_{blood}, \tag{7}$$

where Ht is the haematocrit, F_{RBC} is the volume fraction of erythrocytes in the blood cells and F_{Hb} is the volume fraction of haemoglobin in an erythrocyte. In the present simulation, we assume that these parameters $F_{RBC} = 0.99$, $F_{Hb} = 0.25$ and $Ht = 0.45$ are the same for all the layers [21, 20].

Absorption coefficients of the skin layers The absorption coefficients for seven layers can be described by the spatial distribution of blood vessels, water, glucose, and melanin within the skin tissue [17]:

$$\mu_a(\lambda) = \sum_{i=1}^{n} (\mu_a^{(i)}(\lambda) V_i \prod_{j=1}^{i-1}(1 - V_j)) + \mu^{(0)}(\lambda) \prod_{i=1}^{n}(1 - V_i), \tag{8}$$

where V_i is the volume fraction of the i-th absorber in the given skin layer, n is the total number of absorbers present in the layer, $\mu^{(i)}(\lambda)$ is the absorption coefficient of the i-th absorber, and $\mu^{(0)}(\lambda)$ is the absorption caused by the intrinsic absorption of the layer without any absorbers [13], calculated as:

$$\mu_a^{(0)}(\lambda) = 7.84 \times 10^7 \times \lambda^{-3.255}. \tag{9}$$

The absorption coefficients for blood-free layers, such as stratum corneum and living epidermis [17], are calculated as:

$$\begin{aligned} \mu_a^{(stratum)}(\lambda) = &((0.1 - 0.3 \times 10^{-4}\lambda) \\ &+ 0.125\mu_a^{(0)}(\lambda))(1 - V_w) \\ &+ V_w \mu_a^{(w)}(\lambda), \end{aligned} \tag{10}$$

and

$$\begin{aligned} \mu_a^{(le)}(\lambda) = &(V_{melanin}\mu_a^{(melanin)}(\lambda) \\ &+ (1 - V_{melanin})\mu_a^{(0)}(\lambda))(1 - V_w) \\ &+ V_w \mu_a^{(w)}(\lambda), \end{aligned} \tag{11}$$

where $\mu_a^{(w)}$ and $\mu_a^{(melanin)}$ are the absorption coefficients of water and melanin, respectively. V_w and $V_{melanin}$ are the volume fractions of water and melanin, respectively. The absorption coefficients of the dermal layer $\mu_a^{(dl)}(\lambda)$ and subcutaneous fat layer $\mu_a^{(sf)}(\lambda)$ can be represented by:

$$\begin{aligned} \mu_a^{(dl)}(\lambda) = &(1 - S)V_{Hb}\mu_a^{(Hb)}(\lambda) + SV_{HbO_2}\mu_a^{(HbO_2)}(\lambda) \\ &+ (1 - V_{Hb}V_{blood})(V_{g_{blood}}\mu_a^{(g_{blood})}(\lambda) \\ &+ V_{g_{IF}}\mu_a^{(g_{IF})}(\lambda)) + (1 - V_{Hb}V_{blood}) \\ &(1 - V_{g_{blood}} - V_{g_{IF}})(V_{w_{plasma}}\mu_a^{(w_{plasma})}(\lambda) \\ &+ V_{w_{IF}}\mu_a^{(w_{IF})}(\lambda) + V_{w_{ICF}}\mu_a^{(w_{ICF})}(\lambda)) \\ &+ (1 - V_{Hb}V_{blood})(1 - V_{g_{blood}} - V_{g_{IF}}) \\ &(1 - V_{w_{plasma}} - V_{w_{IF}} - V_{w_{ICF}})\mu_a^{(0)}(\lambda), \end{aligned} \tag{12}$$

and

$$\begin{aligned} \mu_a^{(sf)}(\lambda) = &(1 - S)V_{Hb}\mu_a^{(Hb)}(\lambda) + SV_{HbO_2}\mu_a^{(HbO_2)}(\lambda) \\ &+ (1 - V_{Hb}V_{blood})(V_{g_{blood}}\mu_a^{(g_{blood})}(\lambda)) \\ &+ (1 - V_{Hb}V_{blood})(1 - V_{g_{blood}})(V_{w_{plasma}} \\ &\mu_a^{(w_{plasma})}(\lambda) + V_{w_{IF+ICF}}\mu_a^{(w_{IF+ICF})}(\lambda)) \\ &+ (1 - V_{Hb}V_{blood})(1 - V_{g_{blood}})(1 - V_{w_{plasma}} \\ &- V_{w_{IF+ICF}})\mu_a^{(0)}(\lambda), \end{aligned} \tag{13}$$

where μ_a denotes the wavelength-dependent absorptivity coefficient; $\mu_a^{(Hb)}(\lambda)$, $\mu_a^{(HbO_2)}(\lambda)$, $\mu_a^{(g_{blood})}(\lambda)$, $\mu_a^{(g_{IF})}(\lambda)$, $\mu_a^{(w_{plasma})}(\lambda)$, $\mu_a^{(w_{IF})}(\lambda)$, $\mu_a^{(w_{ICF})}(\lambda)$ $\mu_a^{(w_{IF+ICF})}(\lambda)$ are the absorption coefficients of deoxyhaemoglobin, oxyhaemoglobin, glucose and water, respectively. The calculation of volume fractions can be found in Eq. 3 - 7.

Reduced scattering coefficients of skin layers In the range from visible to short near-infrared wavelengths, the scattering coefficient has a much larger influence than the absorption coefficient on the light propagation in tissue. The reduced scattering coefficients of epidermal layer and the subcutaneous fat layer can be expressed as [14]:

$$\begin{aligned} \mu_s'(\lambda) = &a'(f_{Ray}(\frac{\lambda}{500(nm)})^{-4} \\ &+ (1 - f_{Ray})(\frac{\lambda}{500(nm)})^{-b_{Mie}}), \end{aligned} \tag{14}$$

where the scaling factor a' is 66.7 for the epidermal layer (stratum corneum and living epidermis) and 34.2 for subcutaneous fat; scattering power b_{Mie} is 0.689 for epidermal layer and 0.567 for subcutaneous fat [14]. When glucose concentration is increased in the plasma and IF in the skin layers, the light scattering will be changed because of the mismatch of the index of refraction between the ECF and the membranes of the cells. In our model, we neglect the scattering changes caused by blood cells and other chemical compositions of blood, as previous works suggest that the light scattering is not influenced by red cells and other chemical composition of blood [24, 3]. Furthermore, the glucose concentration in the dermal IF is the closest to the blood glucose concentration based on the research of Groenendaal *et al.* [10]. We assume the reduced scattering coefficient to be affected only by the glucose concentration in the dermal layers, while the scattering coefficients of four layers in the dermal layer are identical. Based on a simple model of scattering dielectric spheres, we can express the reduced scattering coefficient in the dermal layer as [9]:

$$\mu'_{s(dermal)}(\lambda) = 3.28\pi r^2 \rho_s (\frac{2\pi r}{\lambda})^{0.37} (\frac{n_{cell}}{n_{IF}} - 1)^{2.09}, \tag{15}$$

where r is the sphere radius; ρ_s is the volume density of the spheres and n_{cell} and n_{IF} are the refractive indexes of cells and surrounding medium (IF), respectively. As mentioned above, the reduced scattering coefficient of tissues is dependent on the refractive index (n) mismatch between the IF and the cellular components. The increase of glucose concentration in the IF reduces the refractive index mismatch in the dermal layer, hence the reduced scattering coefficient is also reduced:

$$\mu'_{s(dermal)}(\lambda) = 3.28\pi r^2 \rho_s (\tfrac{2\pi r}{\lambda})^{0.37} (\tfrac{n_{cell}}{n_{IF}+\delta n_{glucose}} - 1)^{2.09}, \tag{16}$$

where $\delta n_{glucose}$ is the glucose-induced increase of surrounding medium (IF). The glucose induced change in refractive index is equal to $2.73 \times 10^{-2} M^{-1}$ [25]. Moreover, the reduced scattering coefficient of tissue is also effected by the temperature [15]:

$$\mu'_{s(dermal)}(\lambda) = 3.28\pi r^2 \rho_s (\frac{2\pi r}{\lambda})^{0.37} (\frac{n_{cell}}{n_{IF} + \delta n_{glucose}} - 1)^{2.09} + (4.7e^{-3} \times \Delta T), \tag{17}$$

and

$$\mu'_{s(subcutaneous fat)}(\lambda) = a'(f_{Ray}(\frac{\lambda}{500(nm)})^{-4} + (1 - f_{Ray})(\frac{\lambda}{500(nm)})^{-b_{Mie}}) - (1.4e^{-3} \times \Delta T), \tag{18}$$

where ΔT denotes the increase of temperature.

2.1.2 Modeling results

We will now study the light intensity variations caused by glucose changes as compared to that caused by the changes of body temperature, water concentration and SaO_2. Using the described skin model, our simulation results show that the light intensity is increased by 7.95×10^{-7} when the glucose concentration changes from 0.9 g/l to 1.5 g/l at 660 nm, i.e. the wavelength used in [4]. We also find that (i) 1°C increase of temperature leads to 6.28×10^{-5} decrease of light intensity; (ii) 1% SaO_2 change leads to 2.28×10^{-6} light intensity changes; and (iii) 1% water concentration change leads to 5.28×10^{-8} light intensity changes. Based on the simulation results, we conclude that the light intensity variations caused by temperature and SaO_2 changes can easily interfere that caused by glucose changes at 660 nm.

Since glucose absorption is higher in the short near-infrared range than in the visible range, we perform the same model simulation for the short near-infrared wavelengths. Our model simulation shows that the relative maximum difference in the light intensity is at 970 nm. The light intensity change is 2.23×10^{-5} when glucose concentration increases from 0.9 g/l to 1.5 g/l, which is much larger than that at 660 nm. However, the light intensity change caused by 1% water concentration change is 6.30×10^{-5}, which is larger than that caused by glucose. This is because that the water absorption is the maximum at around 970 nm. Moreover, 1°C temperature change leads to 6.83×10^{-4} light intensity change.

Moreover, we select the wavelength 797 nm in the near-infrared for modeling, which is the isosbestic point for oxyhaemoglobin and deoxyhaemoglobin (i.e. not affected by SaO_2 change) and has low influence of water. The model simulation shows that the light intensity change caused by glucose is 5.01×10^{-6}, which is larger than 8.18×10^{-7} caused by 1% water concentration change. However, 1°C temperature change leads to 2.97×10^{-4} light intensity change, i.e., the effect of temperature is still significant.

Based on the above model simulation on DC measurement, we find that the light intensity change caused by the glucose change can easily be interfered by other factors, especially the change in body temperature.

2.2. AC Component Modeling

The PPG signal contains the light intensity variations from blood volume changes due to pulsating arterial blood. An increase of blood glucose concentration will lead to a change in the PPG amplitude. However, how these glucose-induced amplitude variations relate to the amplitude variations of other absorbers in the visible to near-infrared range are unknown yet. We build a model to simulate the relation between the ratios of PPG amplitudes (i.e., to be independent of the actual pulse-strength) and blood glucose levels. As we mentioned before, the glucose concentration affects

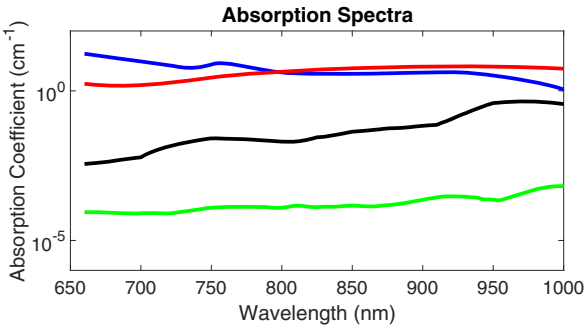

Figure 2. Absorption properties of skin tissues used in the simulation: oxyhaemoglobin (red line), deoxyhaemoglobin (blue line), water (black line) and glucose (green line).

both the absorption and scattering coefficients of arterial blood. It is still unknown how glucose affects the light scattering of blood for *in vivo* glucose measurements, because most current works focus on the analysis of the correlation between light scattering of blood and glucose concentration in *in vitro* experiments. In our model, we focus on studying the changes in light absorption, regardless of the light scattering.

Glucose exhibits several absorption bands in the near-infrared spectrum (700-2500 nm). Within this band, there are strong water absorption band at 1450 nm and 1920 nm [11]. Since we focus on wavelengths within the sensitivity of silicon-based sensors, we limit our analyses to short near-infrared wavelengths (700-1000 nm). The calculation of the PPG amplitude, according to the Beer-Lambert law, can be approximated by:

$$PPG(\lambda) \approx \sum_{i=1}^{n} \varepsilon_i(\lambda) c_i \Delta l_\lambda, \tag{19}$$

where $\varepsilon_i(\lambda)$ is the extinction coefficient of the i-th absorber at the wavelength λ; c_i is the concentration of the i-th absorber in the arterial blood. The Δl_λ is the optical path difference at the wavelength λ due to pulsation. The main absorbers in the blood are oxyhaemoglobin, deoxyhamoglobin and water (see Fig. 2). It can be observed that the absorption coefficients of oxyhaemoglobin, deoxyhamoglobin and water are much larger than glucose in the range $660-1000$ nm. The variations from these three components may easily interfere with the glucose change.

In our model, we simplify the calculation of the PPG amplitude by assuming four absorbers: oxyhaemoglobin, deoxyhaemogblobin, water and glucose, leading to:

$$PPG(\lambda) = (\varepsilon_w(\lambda)c_w + \varepsilon_g(\lambda)c_g + \varepsilon_{HbO2}(\lambda)c_{HbO2} + \varepsilon_{Hb}(\lambda)c_{Hb})\Delta l_\lambda, \tag{20}$$

where ε_w, ε_g, ε_{Hb} and ε_{HbO2} are extinction coefficients of water, glucose, deoxyheamoglobin and oxyhaemoglobin at the wavelength λ, respectively. c_W, c_g, c_{Hb} and c_{HbO2} are the concentrations of water, glucose, deoxyheamoglobin and oxyhaemoglobin, respectively.

We assume that the optical paths at the evaluated wavelengths are equal, so the calculation of the ratio of PPG amplitude is:

$$R = \frac{\varepsilon_w(\lambda_1)c_w + \varepsilon_g(\lambda_1)c_g + \varepsilon_{HbO2}(\lambda_1)c_{HbO2} + \varepsilon_{Hb}(\lambda_1)c_{Hb}}{\varepsilon_w(\lambda_2)c_w + \varepsilon_g(\lambda_2)c_g + \varepsilon_{HbO2}(\lambda_2)c_{HbO2} + \varepsilon_{Hb}(\lambda_2)c_{Hb}}. \tag{21}$$

In this ratio, the wavelength λ_1 is the most glucose-sensitive, resulting in the largest change in PPG amplitude when glucose increases from "Fasting level" to "Maximum glucose level". The wavelength λ_2 has relatively low absorption of glucose, which is selected as the reference wavelength. In the next paragraph we describe how we can estimate the camera-based measurement based on this model.

2.2.1 Model *in vivo* glucose measurement

The above approximation of the PPG amplitude does not take the setup, e.g. camera and illumination, into account. The relative blood volume pulse amplitudes ($\vec{P}_{bv}$) for the different wavelengths of a camera can be calculated by [6]:

$$\vec{P}_{bv}^{c_i} = \frac{\int_{\lambda=400}^{1000} H_{c_i}(\lambda)\frac{I(\lambda)}{I_h(\lambda)} PPG(\lambda) d\lambda}{\int_{\lambda=400}^{1000} H_{c_i}(\lambda)\frac{I(\lambda)}{I_h(\lambda)} \rho_s(\lambda) d\lambda}, \tag{22}$$

where H_{c_i} corresponds to the product of the spectral response of the camera and the response of the applied optical filter of i-th channel; $I(\lambda)$ is the spectrum of the illumination; $I_h(\lambda)$ is the emission spectrum of the tungsten-halogen illumination; $\rho_s(\lambda)$ is the skin reflectance spectrum of the tungsten-halogen illumination. The calculation of the ratio of the normalized blood volume pulse signatures, known as "ratio-of-ratios" commonly used in pulse-oximetry, is as follows:

$$R = \frac{\vec{P}_{bv}^{c_1}}{\vec{P}_{bv}^{c_2}}. \tag{23}$$

2.2.2 Oral Glucose Tolerance Test

In order to induce large variations in glucose, we performed an Oral Glucose Tolerance Test (OGTT), where the camera-based PPG signal was continuously extracted from a forehead region-of-interest (ROI) at four wavelengths in the VIS-NIR range. The experimental setup consisted of four monochrome CCD cameras (AVT Manta G-283B, Allied Vision GmbH, Stadtroda, Germany) equipped with four identical 50 mm lenses and optical bandpass filters with CWLs of 661 nm, 760 nm, 800 nm and 842 nm. The cameras were externally triggered at a stable frame rate of 15 Hz

Predicted ratios	Values
661nm/760nm (blue line)	0.78
661nm/800nm (red line)	0.62
661nm/842nm (yellow line)	0.51
760nm/800nm (purple line)	0.80
760nm/842nm (green line)	0.65
800nm/842nm (turquoise line)	0.81

Table 2. Predicted ratios of relative amplitudes from the model (SaO_2=96%).

Ratios	Changes in ratios caused by Glucose ($\times 10^{-7}$)	Changes in ratios caused by SaO_2 ($\times 10^{-3}$)
661nm/760nm (blue line)	-28.73	-18.26
661nm/800nm (red line)	-13.23	-43.22
661nm/842nm (yellow line)	-2.97	-49.83
760nm/800nm (purple line)	12.58	-12.12
760nm/842nm (green line)	20.57	-15.96
800nm/842nm (turquoise line)	13.25	-3.18

Table 3. Calculated changes in the PPG-amplitude ratios caused by glucose changes and SaO_2 changes.

	661nm/800nm	661nm/842nm
760nm/800nm	0.63	0.71
760nm/842nm	0.64	0.87
800nm/842nm	0.51	0.87

Table 4. Correlation between experimental results.

and were horizontally spaced by 9 cm. The frames from the four cameras were registered using an affine transformation. Illumination was provided by 2 armatures (Falcon Eyes, Hong Kong, China), each equipped with 9 incandescent lamps (Philips 60 W) at a distance of about 1.5 m from the subject. A current-limited DC power supply set to 210 V, 3.95 A (SM330-AR-22, Delta Elektronica, Zierikzee, The Netherlands) powered the lamps. The participant was asked to drink 300 ml water with 75 g glucose within 5 minutes in the morning after overnight fasting. A finger pulse-oximeter was used to measure variations in SaO_2 during the test. The first row of Fig. 3 shows the experimental results during a 120 minutes OGTT. The six lines represent the temporal variations of the possible ratios from the four wavelengths during the OGTT. The average SaO_2 level of the subject is stable, which is measured around 96% during the experiment. The calculated PPG-amplitude ratios between the two wavelength channels, when the SaO_2 level is 96%, are shown in Table 2:

The calculated PPG-amplitude ratios, R, are similar to the experimental results in the Fig. 3. We can see some small deviations between the experimental results and the

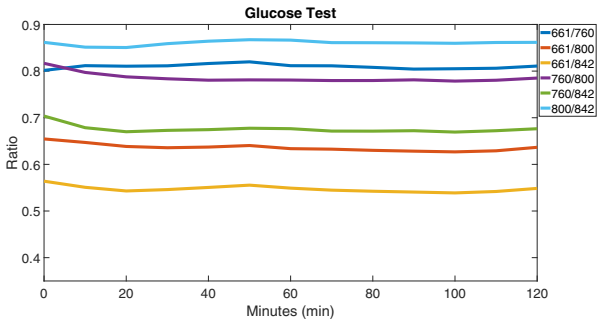

Figure 3. The temporal change of PPG-amplitude ratios measured during the 120 minutes OGTT (661nm/760nm, 661nm/800nm, 661nm/842nm, 760nm/800nm, 760nm/842nm, 800nm/842nm).

simulation results but no major variations. This is to be expected because the changes in PPG-amplitude ratios caused by SaO_2 are small, which can be influenced by the noise from the experimental device (e.g. sensor noise). In general the model simulation is in line with the experimental results.

To investigate whether the small fluctuations are only caused by the changes in SaO_2 during the experiment, we calculated the changes in the PPG-amplitude ratios caused by 1% SaO_2 change and the changes in the PPG-amplitude ratios when glucose increases from 0.9 g/l to 1.5 g/l are shown in the Table 3. The changes in the PPG-amplitude ratios from 661 nm/760 nm, 661 nm/800 nm, and 661 nm/842 nm caused by SaO_2 are different from that caused by glucose.

Moreover, we calculate the correlation between experimental results in Table 4. The PPG-amplitude ratios from 661 nm/760 nm are not used to calculate the correlation, because the PPG-amplitude within this wavelength range is relatively small and thus signal quality is worse, i.e. the correlation is performed for the PPG-signals obtained at longer wavelengths. It shows that the correlation between experimental results is positive, which is contradictory to the simulation results of glucose. It suggests that the fluctuations are more likely to caused by SaO_2 rather than induced by variations in glucose during the experiment.

According to the above simulation results, we observe that even the smallest PPG-amplitude ratio changes (800 nm/842 nm) caused by 1% SaO_2 change is around 774 times larger than the largest PPG-amplitude ratio changes (661 nm/780 nm) caused by glucose change (i.e. when glucose increases from 0.9 g/l to 1.5 g/l). In the next section, we calculate the changes in ratios caused by glucose, SaO_2 and water concentration, to verify the possibility of using the AC component of the PPG waveform for *in vivo* glucose measurement.

2.2.3 Model simulation for short NIR wavelengths

Figure 4 shows that the largest relative PPG-amplitude change is at 700 nm when blood glucose level is raised from "Fasting level" to "Maximum glucose level", and the smallest relative PPG-amplitude change is at 936 nm. Therefore, we selected these two wavelengths to calculate the ratio of relative pulse amplitudes R. This ratio increases by 1.87×10^{-6} when glucose increases from 0.9 g/l to 1.5 g/l. We also find that the changes in ratios caused by 1% SaO_2 change is 1.33×10^{-2}, caused by 1% water concentration change is 4.60×10^{-5}. Consequently, the variations in SaO_2 create significant interference for *in vivo* glucose measurement in short near-infrared wavelengths, rendering the feasibility of PPG-based glucose monitoring unlikely, especially for the generally more noise camera PPG signals.

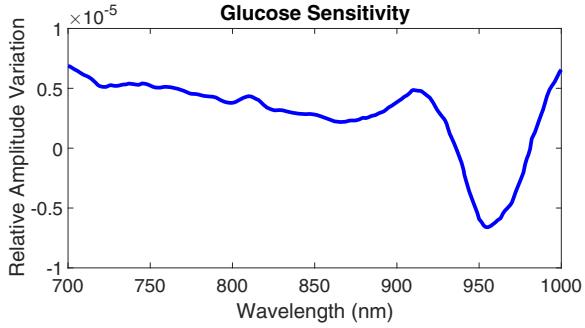

Figure 4. The relative change in PPG amplitude when the glucose changes from 0.9 g/l to 1.5 g/l for the short near-infrared wavelengths.

2.3. Future work

In this paper we focus on elaborating the theoretical possibility of camera-based glucose monitoring by mathematical modeling. A set of preliminary tests are conducted to verify our hypothesis and expectations as the first step. As for the future work, we shall implement a thorough experiment/benchmark to further conclude the feasibility of camera-based glucose monitoring.

3. Conclusion

In this paper we investigated the theoretical feasibility of remote glucose measurement with a regular camera by modeling. Model simulations based on the DC component suggest the glucose-induced intensity variations are so small that even the effect of body temperature changes are larger. For the AC component, the light intensity variations caused by glucose changes are easily masked by even minute SaO_2 changes due to the high absorption and concentration of (oxy-)hemoglobin. Our study shows that it is unlikely to measure the blood glucose levels using a regular silicon-based camera in the range of visible and short near-infrared wavelengths.

References

[1] M. Aloraefy, T. J. Pfefer, J. C. Ramella-Roman, and K. E. Sapsford. In vitro evaluation of fluorescence glucose biosensor response. *Sensors*, 14(7):12127–12148, 2014. 1

[2] A. Canavan and B. S. Arant Jr. Diagnosis and management of dehydration in children. *children*, 100(17):18–19, 2009. 2

[3] O. Cohen, I. Fine, E. Monashkin, and A. Karasik. Glucose correlation with light scattering patternsa novel method for non-invasive glucose measurements. *Diabetes technology & therapeutics*, 5(1):11–17, 2003. 4

[4] V. Dantu. Derivative spectroscopy in non-invasive blood-glucose analysis. In *Connected Health: Applications, Systems and Engineering Technologies (CHASE), 2016 IEEE First International Conference on*, pages 350–351. IEEE, 2016. 1, 2, 4

[5] V. Dantu, J. Vempati, and S. Srivilliputhur. Non-invasive blood glucose monitor based on spectroscopy using a smartphone. In *Engineering in Medicine and Biology Society (EMBC), 2014 36th Annual International Conference of the IEEE*, pages 3695–3698. IEEE, 2014. 1, 2

[6] G. de Haan and A. van Leest. Improved motion robustness of remote-ppg by using the blood volume pulse signature. *Physiological Measurement*, 35(9):1913, 2014. 5

[7] D. T. Delpy, M. Cope, P. van der Zee, S. Arridge, S. Wray, and J. Wyatt. Estimation of optical pathlength through tissue from direct time of flight measurement. *Physics in medicine and biology*, 33(12):1433, 1988. 2

[8] I. Federation. Idf diabetes atlas 6th, 2015. 1

[9] H. B. Ganzeboom, P. M. De Graaf, and D. J. Treiman. A standard international socio-economic index of occupational status. *Social science research*, 21(1):1–56, 1992. 4

[10] W. Groenendaal, G. von Basum, K. A. Schmidt, P. A. Hilbers, and N. A. van Riel. Quantifying the composition of human skin for glucose sensor development, 2010. 4

[11] K. H. Hazen, M. A. Arnold, and G. W. Small. Measurement of glucose in water with first-overtone near-infrared spectra. *Applied Spectroscopy*, 52(12):1597–1605, 1998. 5

[12] M. Hiraoka, M. Firbank, M. Essenpreis, M. Cope, S. Arridge, P. Van Der Zee, and D. Delpy. A monte carlo investigation of optical pathlength in inhomogeneous tissue and its application to near-infrared spectroscopy. *Physics in medicine and biology*, 38(12):1859, 1993. 2

[13] P. F. Jacques, A. G. Bostom, R. R. Williams, R. C. Ellison, J. H. Eckfeldt, I. H. Rosenberg, J. Selhub, and R. Rozen. Relation between folate status, a common mutation in methylenetetrahydrofolate reductase, and plasma homocysteine concentrations. *Circulation*, 93(1):7–9, 1996. 3

[14] S. L. Jacques. Optical properties of biological tissues: a review. *Physics in medicine and biology*, 58(11):R37, 2013. 3, 4

[15] J. Laufer, R. Simpson, M. Kohl, M. Essenpreis, and M. Cope. Effect of temperature on the optical properties of ex vivo human dermis and subdermis. *Physics in Medicine and Biology*, 43(9):2479, 1998. 4

[16] S. L. Lewis, L. Bucher, M. M. Heitkemper, M. M. Harding, J. Kwong, and D. Roberts. *Medical-surgical nursing: assessment and management of clinical problems, single volume*. Elsevier Health Sciences, 2016. 1

[17] I. V. Meglinski and S. J. Matcher. Quantitative assessment of skin layers absorption and skin reflectance spectra simulation in the visible and near-infrared spectral regions. *Physiological measurement*, 23(4):741, 2002. 2, 3

[18] E. Monte-Moreno. Non-invasive estimate of blood glucose and blood pressure from a photoplethysmograph by means of machine learning techniques. *Artificial intelligence in medicine*, 53(2):127–138, 2011. 1

[19] E. A. Moschou, B. V. Sharma, S. K. Deo, and S. Daunert. Fluorescence glucose detection: advances toward the ideal in vivo biosensor. *Journal of fluorescence*, 14(5):535–547, 2004. 1

[20] V. Priezzhev, E. Ivashkevich, A. Povolotsky, and C.-K. Hu. Exact phase diagram for an asymmetric avalanche process. *Physical review letters*, 87(8):084301, 2001. 2, 3

[21] E. M. Renkin. *Handbook of physiology: Section 2, The cardiovascular system. Microcirculation: pt. 2*, volume 4. American Physiological Soc., 1984. 3

[22] K. Sakamoto, F. Kubo, K. Yoshiuchi, A. Ono, T. Sato, K. Tomita, K. Sakaguchi, M. Matsuhisa, H. Kaneto, H. Maegawa, et al. Usefulness of a novel system for measuring glucose area under the curve while screening for glucose intolerance in outpatients. *Journal of diabetes investigation*, 4(6):552–559, 2013. 1

[23] C.-F. So, K.-S. Choi, T. K. Wong, and J. Chung. Recent advances in noninvasive glucose monitoring. *Medical Devices: Evidence and Research*, 2012. 1

[24] S. V. Tsinopoulos, E. J. Sellountos, and D. Polyzos. Light scattering by aggregated red blood cells. *Applied optics*, 41(7):1408–1417, 2002. 4

[25] V. V. Tuchin, I. L. Maksimova, D. A. Zimnyakov, I. L. Kon, A. H. Mavlutov, and A. A. Mishin. Light propagation in tissues with controlled optical properties. *Journal of biomedical optics*, 2(4):401–417, 1997. 4

[26] S. K. Vashist. Non-invasive glucose monitoring technology in diabetes management: A review. *Analytica chimica acta*, 750:16–27, 2012. 1

[27] G. S. Wilson and Y. Zhang. *Introduction to the Glucose Sensing Problem*, pages 1–27. John Wiley & Sons, Inc., 2009. 1

[28] H. Zeller, P. Novak, and R. Landgraf. Blood glucose measurement by infrared spectroscopy. *The International Journal of Artificial Organs*, 12(2):129–135, 1989. PMID: 2707907. 1